Wave-function engineering and absorption spectra in Si 0.16 Ge 0.84 /Ge 0.94 Sn 0.06 /Si 0.16 Ge 0.84 strained on relaxed Si 0.10 Ge 0.90 type I quantum well

N. Yahyaoui, N. Sfina, J.-L. Lazzari, A. Bournel, M. Said

AIP | Journal of Applied Physics

Wave-function engineering and absorption spectra in Si0.16Ge0.84/Ge0.94Sn0.06/Si0.16Ge0.84 strained on relaxed Si0.10Ge0.90 type I quantum well

N. Yahyaoui, N. Sfina, J.-L. Lazzari, A. Bournel, and M. Said

Citation: Journal of Applied Physics **115**, 033109 (2014); doi: 10.1063/1.4862226
View online: http://dx.doi.org/10.1063/1.4862226
View Table of Contents: http://scitation.aip.org/content/aip/journal/jap/115/3?ver=pdfcov
Published by the AIP Publishing

Wave-function engineering and absorption spectra in $Si_{0.16}Ge_{0.84}/Ge_{0.94}Sn_{0.06}/Si_{0.16}Ge_{0.84}$ strained on relaxed $Si_{0.10}Ge_{0.90}$ type I quantum well

N. Yahyaoui,[1,a)] N. Sfina,[1] J.-L. Lazzari,[2] A. Bournel,[3] and M. Said[1,a)]
[1]*Laboratoire de la Matière Condensée et des Nanosciences (LMCN), Département de Physique, Faculté des Sciences de Monastir, Avenue de l'Environnement, 5019 Monastir, Tunisia*
[2]*Centre Interdisciplinaire de Nanoscience de Marseille (CINaM), UMR CNRS 7325, Aix-Marseille Université, Case 913, Campus de Luminy, 13288 Marseille cedex 9, France*
[3]*Institut d'Electronique Fondamentale (IEF), UMR CNRS 8622, Université Paris-Sud, Bât. 220, 91405 Orsay cedex, France*

(Received 16 November 2013; accepted 2 January 2014; published online 17 January 2014)

We theoretically investigate germanium-tin alloy as a semiconductor for the design of near infrared optical modulators in which the $Ge_{1-x}Sn_x$ alloy is the active region. We have calculated the electronic band parameters for heterointerfaces between strained $Ge_{1-x}Sn_x$ and relaxed $Si_{1-y}Ge_y$. Then, a type-I strain-compensated $Si_{0.10}Ge_{0.90}/Si_{0.16}Ge_{0.84}/Ge_{0.94}Sn_{0.06}$ quantum well heterostructure optimized in terms of compositions and thicknesses is studied by solving Schrödinger equation without and under applied bias voltage. The strong absorption coefficient ($>1.5 \times 10^4\,cm^{-1}$) and the shift of the direct transition under large Stark effect at 3 V are useful characteristics for the design of optoelectronic devices based on compressively strained IV-IV heterostructures at near infrared wavelengths. © *2014 AIP Publishing LLC*.
[http://dx.doi.org/10.1063/1.4862226]

I. INTRODUCTION

Germanium, which is a group IV material, has unique properties associated with the presence of a strong dipole-allowed direct transition. The energy gap between the top of the valence band and the conduction has a local minimum at the Γ point, which is only 0.14 eV above its fundamental indirect band edge at room temperature. In addition, due to the small difference between direct and indirect band gap energy, Ge appeared to be a promising material for next generation on-chip light sources and detectors[1,2] and thus triggered a lot of activities for photonic applications.[3–7] Thereby, the main issue is to overcome the inefficient light emission of an indirect semiconductor. Therefore, several solutions attempts have been proposed to introduce tensile strain in Ge thin films such as micromechanical strain[8–10] and epitaxial growth of Ge on larger lattice constant buffer layers. Recently, Kuo and co-workers[11] demonstrated that the direct E_0 transition in Ge can be tuned via quantum confinement in much the same way as in direct gap materials, despite the fact that electrons at the Γ-minimum can, in principle, relax to the lower-energy indirect valleys at the *L*-points of the Brillouin zone (BZ). This breakthrough opened up important applications in the field of modulators monolithically integrated to silicon platforms. Another approach, substitution of α-Sn into Ge lattice to form semiconducting GeSn alloy has also been found to result in an effect similar to that observed in Ge under tensile strain, i.e., lowering in energy of the direct valley below the indirect.[12] Also, the recent experimental investigations of Ref. 13 demonstrated the lowering of E_0 as a function of the α-Sn concentration and the expected reduction of the direct-indirect separation. For small amounts of α-Sn ranging from 6% to 11%, the alloy is predicted to undergo an indirect to direct transition.[14–16] Besides the tunable direct gap, GeSn alloy system has also been predicted to exhibit high electron and hole mobilities,[17] making it an ideal material platform for co-integration of optoelectronic and high speed electronic devices.[18,19] Recently, high-quality binary GeSn and ternary SiGeSn alloys with high-Sn composition have been successfully synthesized,[20,21] making it possible to create new photonic devices based on the SiGeSn material system, such as lasers,[22–26] modulators,[27] and detectors,[28–30] for electronic-photonic integrated circuits. Chang and Chang proposed in a recent paper a polarization-insensitive waveguide modulator at 1.55 μm using a Ge/SiGeSn multiple-quantum-well (MQW) structure and analyzed its operation at room-temperature.[31]

For the same aim, and based on our previous work on SiGe/Ge/SiGe heterostructures,[32] we propose a simulation of a silicon-based optical modulator operating at 1.55 μm, in which the Ge active region has been substituted by a GeSn quantum well (QW). The alloy compositions were chosen to fulfil three conditions simultaneously: a type-I band alignment between $Ge_{1-x}Sn_x$ and $Si_{0.16}Ge_{0.84}$, a direct transition in the GeSn quantum well, and an improved quantum confinement in the $Ge_{1-x}Sn_x$ conduction and valence bands. In order to design such device, it is very important to determine the electronic properties of strained GeSn, such as band gap energy and bands discontinuities as a function of composition. In a first step toward the calculation of optical properties of GeSn quantum-well, we report the band offsets at $Ge_{1-x}Sn_x/Si_{1-y}Ge_y$ strained/(001)-oriented relaxed interfaces

[a)]Authors to whom correspondence should be addressed. Electronic addresses: naima.yahyaoui@yahoo.fr and moncef_said@yahoo.fr

as well as the effective masses deduced from $k\cdot p$ strained Hamiltonian. Then, we investigate the Stark effect on the quantized subbands and the absorption coefficient spectrum. The effects of the bias voltage at room temperature are finally presented and discussed.

II. CALCULATION OF MATERIAL PARAMETERS

Energy-band theory and photoluminescence experiments[15,33] have indicated that the band gap of $Ge_{1-x}Sn_x$ alloys makes a transition from indirect to direct. This transition occurs at $x = 0.06$–0.11.[14–16] In this work, we adjusted the pseudo potential form factors to fit the experimental band energies of Ge and α-Sn. The electronic band structure is calculated using the empirical pseudo potential (EPM) within the virtual crystal approximation (VCA) combined with the bond-orbital model of Harrison.[34] Since both Ge and α-Sn crystallize in the diamond structure, their antisymmetric form factors are zero. Hence, it remains only the symmetric form factors for the $Ge_{1-x}Sn_x$ alloys, which can be obtained according to the following expressions:

$$V^S_{Ge_{1-x}Sn_x} = (1-x)V^S_{Ge} + xV^S_{Sn}. \quad (1)$$

For $Ge_{1-x}Sn_x$ alloys, the lattice constant has been assumed to be described by

$$a_{Ge_{1-x}Sn_x} = (1-x)a_{Ge} + xa_{Sn} + \theta_{GeSn}x(1-x), \quad (2)$$

where $\theta_{GeSn} = 0.166$ Å.

Using this lattice constant, the corresponding reciprocal lattice vectors and the pseudo potential form factors $V^S(G)$of Eq. (1), we can calculate the band structures of $Ge_{1-x}Sn_x$ alloys. Moreover, the VCA approximation does not take into account the effect of compositional disorder and hence the bowing factors obtained by VCA may deviate from experiments.[35,36] In order to overcome this shortcoming, we have added to the VCA a non-periodic potential due to the compositional disorder.[37] By adding this disorder effective potential to the virtual crystal potential, the expression (1) becomes

$$V^S_{Ge_{1-x}Sn_x} = (1-x)V^S_{Ge} + xV^S_{Sn} - p[x(1-x)]^{\frac{1}{2}}[V^S_{Sn} - V^S_{Ge}], \quad (3)$$

p is then treated as an adjustable parameter.

The final adjusted pseudopotential form factors of Ge and α-Sn are summarized in Table I. The calculated direct and indirect band gap energies of relaxed $Ge_{1-x}Sn_x$ at Γ and L high-symmetry points in the BZ using the EPM under the VCA are shown in Figure 1(a) and fitted to second order equation in alloy α-Sn composition x

$$E_g^{(\Gamma)}(x) = 0.782 - 1.734x + 0.94x^2, \quad (4)$$

$$E_g^{(L)}(x) = 0.688 - 0.15x - 0.25x^2. \quad (5)$$

The unit of the energy is eV. The band gap bowing factors are $b_\Gamma \sim 0.94$ eV and $b_L \sim -0.25$ eV in Eqs. (4) and (5). By varying x from 0 to 0.2, the band gap reduction at Γ-point ($E_{g,\,\Gamma}$) is more pronounced than that at L-point ($E_{g,\,L}$), causing $Ge_{1-x}Sn_x$ alloy to become a direct band-gap material when x is 0.057 or larger. At $x = 0.057$, the band gap energy at Γ and L points are crossing. Comparison of the calculated direct and indirect band gap with the experimental data measured at 300 K (Ref. 38) is also shown in Figure 1(a). This can be observed from a comparison between the full band structures of $Ge_{1-x}Sn_x$ with $x = 0$ and $x = 0.06$ as shown in Figure 1(b).

In order to perform a simulation of the optoelectronic characteristics of $Ge_{1-x}Sn_x$ near-infrared optical modulators, material parameters of $Ge_{1-x}Sn_x$ such as discontinuities in valence and conduction bands as well as effective masses are needed. The band offsets between binary α-Sn containing alloys and Si or Ge are not known experimentally,[25] we have adopted the procedure outlined by Yahyaoui *et al.* in Ref. 32 using the parameters taken form Refs. 15 and 22 and listed in Table II. The conduction and valence-band discontinuities between the $Ge_{1-x}Sn_x$ strained layer and the (001)-oriented relaxed $Si_{1-y}Ge_y$ substrate are calculated thanks to these data. The results of conduction band offsets are plotted in Figure 2(a), at Γ and L points, respectively. Figure 2(b) shows the valence band offsets for heavy and light holes. For a strained $Ge_{1-x}Sn_x$ on relaxed $Si_{0.1}Ge_{0.9}$ heterointerface, the following approximated analytical laws of the conduction and valence-band discontinuities between strain splitted valleys are given below in (6), (7), (8), and (9):

$$\Delta E_C{}^{\Gamma}(x) \cong -0.353 - 1.0654x + 1.875x^2, \quad (6)$$

$$\Delta E_C{}^{L}(x) \cong -0.1 - 0.1223x + 0.91157x^2, \quad (7)$$

$$\Delta E_{v,hh}(x) \cong 0.1158 + 1.3382x - 0.0904x^2, \quad (8)$$

$$\Delta E_{v,lh}(x) \cong 0.092 + 1.03x - 0.085x^2. \quad (9)$$

Next, we have calculated the strained band-gap energies versus the composition x for $Ge_{1-x}Sn_x$ strained layer on relaxed $Si_{0.1}Ge_{0.9}$ and Ge substrates. The GeSn/$Si_{0.1}Ge_{0.9}$ (001) alloy may have a direct band gap at Sn-fractions higher than 20% at room temperatures. Regarding the pseudomorphic $Ge_{1-x}Sn_x$/Ge, the indirect-to-direct crossover may occur at a Sn-fraction of 15.3% at 300 K. The latter value is consistent with the experimental crossover found at about 17% in Ref. 21; our theoretically determined values are plotted in Figure 1(a). The analytical expressions are quoted as follows:

$$E_g^{(\Gamma-hh)}(x) = 0.828 - 2.34x + 1.96538x^2, \quad (10)$$

TABLE I. Pseudo potential parameters for Ge and α-Sn used in EPM.

	Form factors (Ry)			Band gap energies (eV)	
Material	V_s (3)	V_s (8)	V_s (11)	E_g^Γ	E_g^L
Ge	−0.299088	0.075200	0.001723	0.79[a]	0.69[a]
				0.8[b]	0.66[b]
α-Sn	−0.195	−0.008	0.04	0.00[a]	0.28[a]
				−0.41[b]	0.14[b]

[a]Present work.
[b]Reference 25.

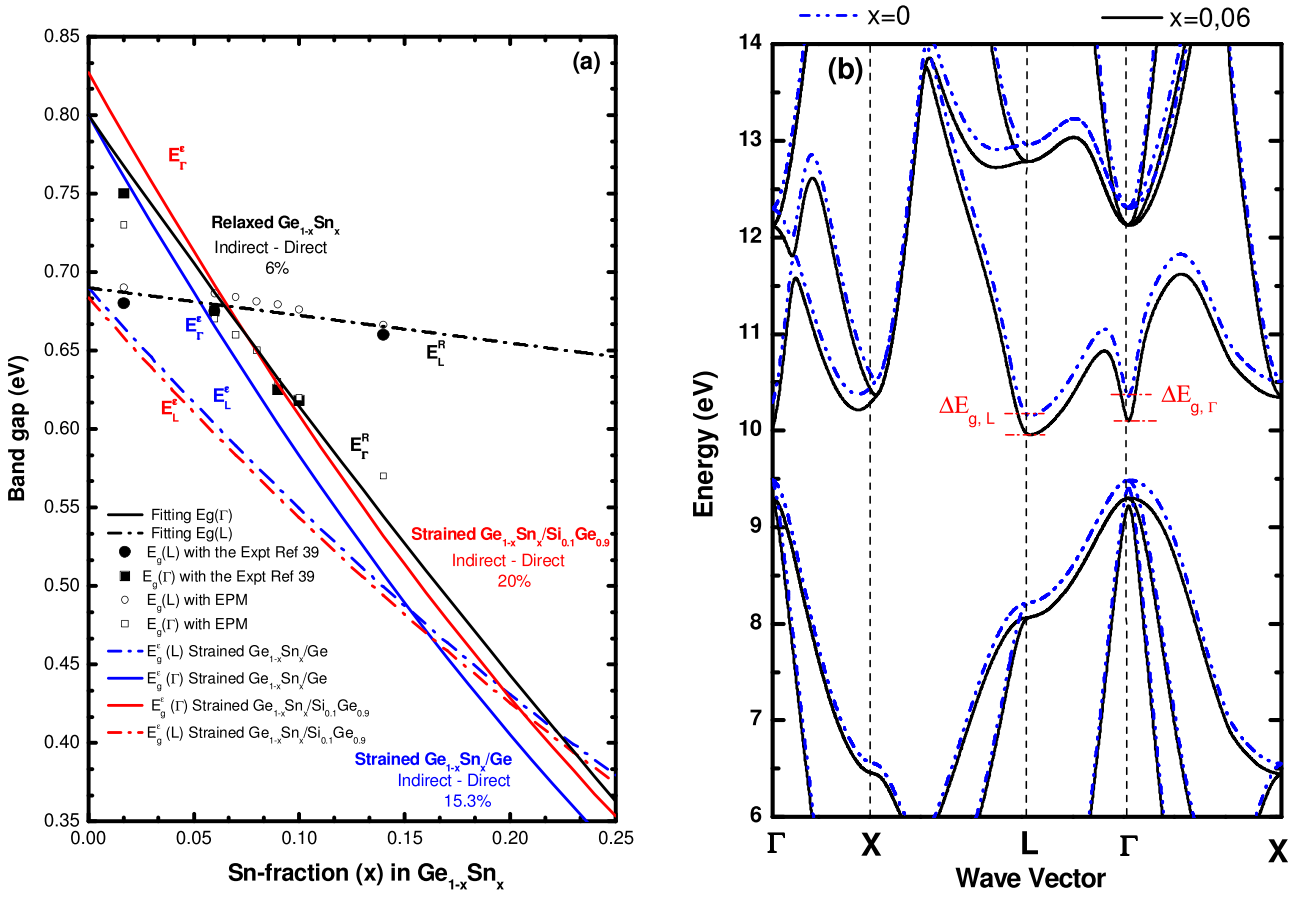

FIG. 1. (a) Composition dependence of energy band gaps at Γ- and L-valleys for relaxed and strained $Ge_{1-x}Sn_x$, respectively. For $Ge_{1-x}Sn_x$ alloys with Sn composition x below 0.057, the conduction band minimum is at L-point, and the alloy is an indirect band-gap material. Symbols are experimental data and the black lines are obtained from EPM calculation. For strained $Ge_{1-x}Sn_x$ on relaxed Ge (blue color) and $Ge_{1-x}Sn_x$ on relaxed $Si_{0.1}Ge_{0.9}$ (red color), the crossover indirect-direct band gaps (E_L^e and E_Γ^e) are at 15.3% and 20%, respectively. (b) Full band E-k dispersion for $Ge_{1-x}Sn_x$ with x = 0 and x = 0.06. The differences in band-gaps at Γ-point and L-point are highlighted as $\Delta E_{g,\Gamma}$ and $\Delta E_{g,L}$.

$$E_g^{(\Gamma-lh)}(x) = 0.8433 - 2.086x + 1.9602x^2, \quad (11)$$

$$E_g^{(L-hh)}(x) = 0.679 - 1.464x + 1.0033x^2, \quad (12)$$

$$E_g^{(L-lh)}(x) = 0.694 - 1.1574x + 0.998x^2, \quad (13)$$

with energies given in eV.

Another key parameter is the effective mass which governs the electron transport in semiconductor devices. Unfortunately, experimental effective masses for the dilute alloys are not known in the literature and thus we need to employ estimated masses. We shall use the strained Hamiltonian k·p at the center of the high symmetry point Γ.[39] The in-plane effective masses for electron, heavy-hole, and light-hole bands, respectively, can be calculated using equations outlined in Refs. 39 and 40. The effective mass is obtained by calculation of the energy E versus wave vector (k) relation

$$E_j(K) = \frac{\hbar^2 k^2}{2m_j^*}\left(1 - \gamma_j{}^2 k^2\right), \quad (14)$$

where the effective mass is m_j^* and γ_j is the nonparabolicity parameter for the j band.

One obtains for the strain-dependent hole effective masses

$$m_{hh}^{\perp} = \frac{1}{\gamma_1 - 2\gamma_2}, \quad (15)$$

$$m_{\substack{j=lh \\ j=so}}^{\perp} = \frac{2E_j + \Delta_0 + \varepsilon}{2E_j(\gamma_1 + \gamma_2) + \Delta_0(\gamma_1 + 2\gamma_2) - \varepsilon(8\gamma_2 - \gamma_1)}, \quad (16)$$

TABLE II. Band parameters at 300 K for Si, Ge, and α-Sn used for the calculations:[15,22] lattice constant a (in Å), elastic stiffness constants c_{11} and c_{12} (in 10^{12} dyn cm^{-2}), Kohn-Luttinger parameters γ_1 and γ_2, valence-band averaged energy $E_{v,av}$, spin-orbit splitting Δ_0, and deformation potentials b, a_c, and a_v (in eV).

	a	c_{11}	c_{12}	$E_{v,av}$	Δ_0	b	a_c	a_v	γ_1	γ_2
Si	5.4311	1.675	0.650	−0.47	0.04	−2.1	1.98	2.46	4.22	0.39
Ge	5.6579	1.315	0.494	0	0.30	−2.9	−8.24	1.24	13.38	4.24
α−Sn	6.4892	6.9	2.9	0.69	0.80	−2.7	−5.33	1.55	−15	−11.45

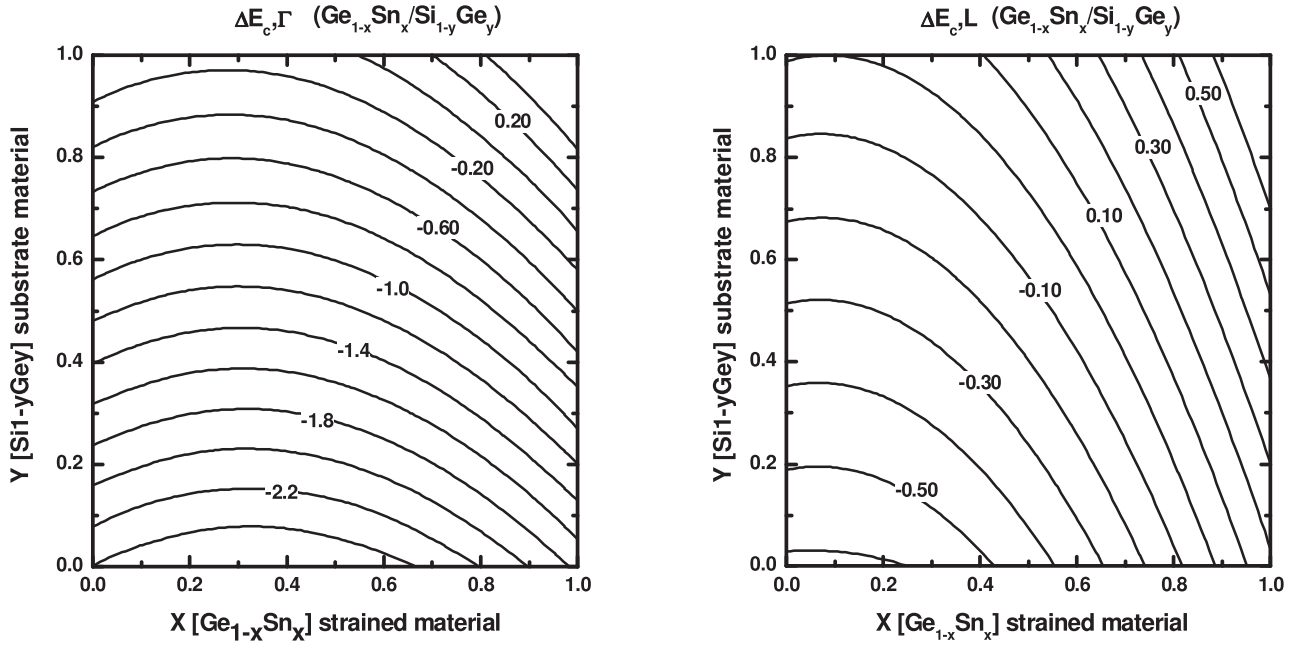

(a)

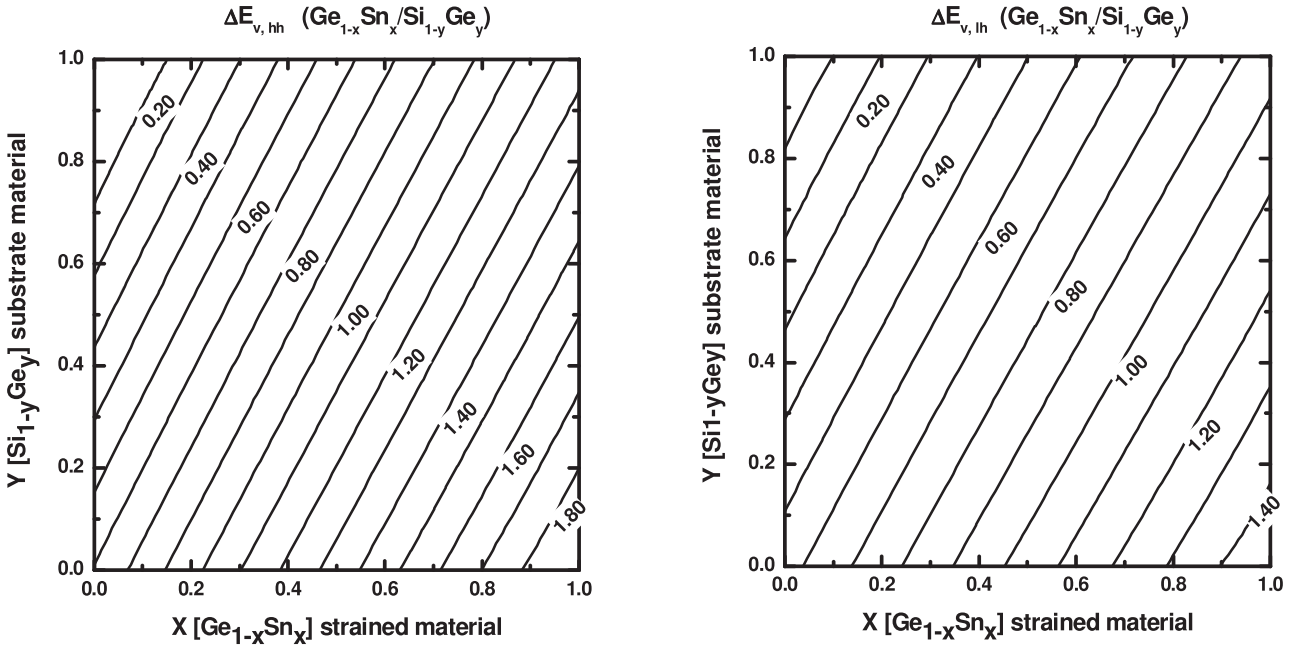

(b)

FIG. 2. (a) Conduction-band offsets $E_c(x)$-$E_c(y)$ at the minimum Γ and L points. (b) Valence band offsets for heavy holes and light holes for the $Ge_{1-x}Sn_x/Si_{1-y}Ge_y$ heterointerfaces. All values are expressed in eV.

$$m_{hh}^{//} = \frac{1}{\gamma_1 + \gamma_2}, \tag{17}$$

$$m_{\substack{j=lh \\ j=so}}^{//} = \frac{(\varepsilon - E_j)(\varepsilon + E_j) + (\varepsilon - E_j)(\Delta_0 + E_j) - \left[(\varepsilon + E_j)(\Delta_0 + E_j) - 2\varepsilon^2\right]}{\gamma_1(\varepsilon - E_j)(\varepsilon + E_j) + (\gamma_1 - \gamma_2)(\varepsilon - E_j)(\Delta_0 + E_j) - (\gamma_1 + \gamma_2)\left[(\varepsilon + E_j)(\Delta_0 + E_j) - 2\varepsilon^2\right] + 4\varepsilon\gamma_2(\varepsilon - E_j)}, \tag{18}$$

with

$$E_{j=hh} = -\frac{1}{2}\delta E_{001}, \tag{19}$$

$$E_{j=lh} = -\frac{1}{2}\Delta_0 + \frac{1}{4}\delta E_{001} + \frac{1}{2}\left[\Delta_0^2 + \Delta_0\delta E_{001} + \frac{9}{4}(\delta E_{001})^2\right]^{\frac{1}{2}}, \quad (20)$$

$$E_{j=so} = -\frac{1}{2}\Delta_0 + \frac{1}{4}\delta E_{001} - \frac{1}{2}\left[\Delta_0^2 + \Delta_0\delta E_{001} + \frac{9}{4}(\delta E_{001})^2\right]^{\frac{1}{2}}, \quad (21)$$

$$\varepsilon = -\frac{1}{2}\delta E_{001} = -b(\varepsilon_{\perp} - \varepsilon_{//}). \quad (22)$$

The effective mass of the conduction electrons at the Γ-point minimum may be written as[41]

$$\frac{m}{m_{c\Gamma}} = 1 + \frac{2P^2}{3m}\left(\frac{2}{E_0} + \frac{1}{E_0 + \Delta_0}\right). \quad (23)$$

As for the matrix element P, the following expression is used:

$$\frac{P^2}{m}(y) = 12.6eV\left[\frac{a_{Ge}}{a(y)}\right]^2. \quad (24)$$

This reproduces the electron effective mass in pure Ge.

Constant values and the meaning of the parameters used are summarized in Table II. The effective masses for Γ and L electrons, heavy hole, and light hole, respectively, are illustrated in Figure 3 for $Ge_{1-x}Sn_x/Si_{1-y}Ge_y$ calculated versus α-Sn compositions. All results are given in units of the free electron mass m_0. Electron effective masses at L and Γ-points and the hh effective masses of $Ge_{1-x}Sn_x$ decrease slightly with increasing Sn composition, whereas, the lh

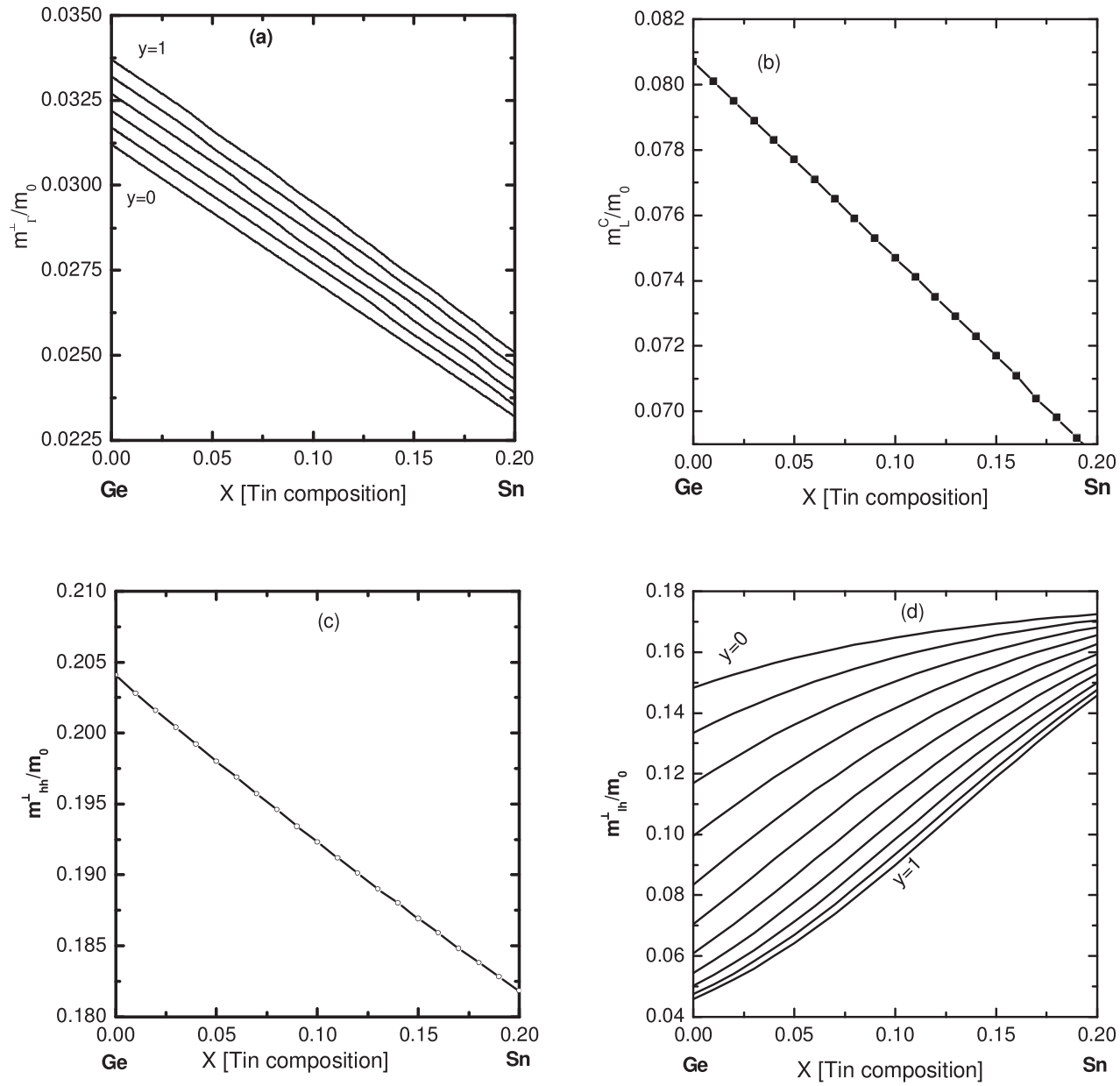

FIG. 3. Transverse electron effective masses at Γ-point (a) and at L-point (b). Perpendicular heavy holes (c) and light holes (d) effective masses of strained $Ge_{1-x}Sn_x$ on a relaxed $Si_{1-y}Ge_y$ substrate as function of α-Sn composition. All results are given in units of the free electron mass m_0.

effective masses of $Ge_{1-x}Sn_x$ increase significantly and then decrease a bit with increasing x.

III. SIMULATION AND ABSORPTION SPECTRA

Using the above results, we have simulated the conduction and valence bands edges of the considered heterostructure. The proposed stacks are designed in a pragmatic way for a pseudomorphic growth on relaxed $Si_{0.9}Ge_{0.1}$ assuming individual layer thickness being smaller than the known critical thickness and an overall compensation of the strain.[42] Our modeled structure consists of $Ge_{0.94}Sn_{0.06}$ QW separated by two $Si_{0.16}Ge_{0.84}$ barriers, for the strained part of the structure, the whole is embedded between (001)-oriented relaxed $Si_{0.10}Ge_{0.90}$. These compositions of GeSn and SiGe are chosen in such a way that they form type-I band alignment, ensure the direct interband transitions and an improved quantum confinement of electrons and holes. Moreover, the low solid solubility[43] (<1%) of Sn in Ge makes very difficult the growth of high quality, defect free GeSn. However, recent advances in non-equilibrium growth techniques[44] have made possible to achieve GeSn alloy with substitutional Sn content exceeding 8%. Nevertheless, increasing Sn % in the alloy raises concerns regarding thermal stability of the material and the maximum allowable thermal budget during device fabrication as pointed out by recent investigations of Ref. 45.

The line-up of various relevant bands of a SiGe/GeSn QW is illustrated in Figure 4. We show the conduction band edge at the L-point ($E_{c,L}$) and at the Γ point ($E_{c,\Gamma}$), as well as the valence band edges corresponding to the heavy hole ($E_{v,hh}$) and light hole ($E_{v,lh}$) bands. The corresponding offsets for the conduction band at the L ($\Delta E_{c,L}$) and the Γ ($\Delta E_{c,\Gamma}$), and for the heavy hole ($\Delta E_{v,hh}$) and the light hole ($\Delta E_{v,lh}$) are also shown. The quantum confinement leads to energy subbands in both conduction and valence bands. The energy levels of these subbands can be calculated by solving the one-dimensional Schrödinger equation following the envelope function approximation.[42] Figure 5 shows simulation of the band diagram, hole and electron wave functions of the $Ge_{0.94}Sn_{0.06}$ quantum well. We find that $Ge_{0.94}Sn_{0.06}/Si_{0.16}Ge_{0.84}$ quantum well on relaxed $Si_{0.1}Ge_{0.9}$ has type-I alignment. From symmetry, we expect to observe the interband transition series consisting of hh_1-e_1, lh_1-e_1, hh_2-e_2, lh_2-e_2, etc., where hh_n, lh_n, and e_n denote the nth heavy hole, light hole, and electron states at the Γ (at the L) edge, respectively. We find that the hh_1-cΓ_1 transition energy is equal to 0.977 eV. For better comparison, we calculated the interband absorption spectrum associated with the generation of an electron-hole pair in the $Ge_{0.94}Sn_{0.06}$ quantum well using the following theoretical method. The theoretical dispersion of the absorption coefficient is obtained from the imaginary and real parts of the estimated dielectric constant, respectively. In the estimation of the free-carrier contribution, energy-and polarization-dependent momentum matrix elements[46] and line broadening represented by a Gaussian line shape function were taken into account. The contribution of free-carrier-transitions to the imaginary part may be written as

$$\alpha(\hbar\omega) = \frac{e^2}{\varepsilon_0 m_0^2 L_{eff}} \frac{m_{eh}}{\Pi\hbar^2} \sum_i \sum_j |M_b|^2 \left| \int \Psi_{ei}(z)\Psi_{hj}(z)dz \right|^2 \times \int M(E)F(E + E_g + E_{ei} + E_{hj} - \hbar\omega)dE. \quad (25)$$

Here, L_{eff} is the thickness of the QW; m_{eh} is the reduced hole effective mass; E_g, E_{ei}, and E_{hj} are the energy gap; the quantized energies of the i electron and j hole, respectively; and $\hbar\omega$ denotes the photon energy. The energies E_{ei} and E_{hj}, and the related wave functions, $\Psi_{ei}(z)$ and $\Psi_{hj}(z)$, are solutions of the one-dimensional Schrödinger equations for the QW subjected to the electric field.[47] The quantity $|M_b|^2$ is the average matrix element for the Bloch state[48] given by

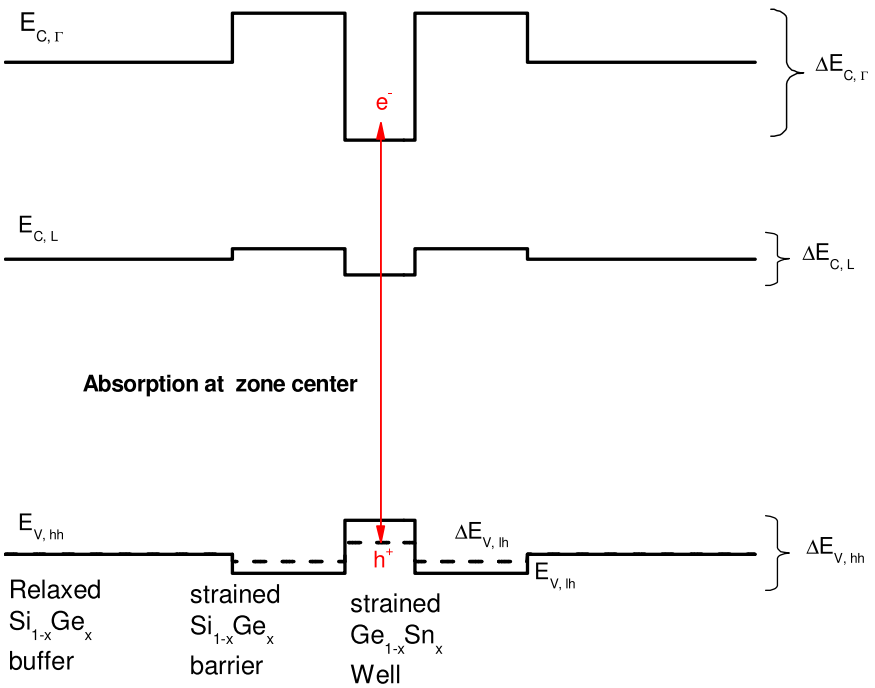

FIG. 4. Band structures along the considered GeSn/SiGe heterostructure. $E_{c,\Gamma}$ and $E_{c,L}$ are the energies of the bottom of the conduction band at zone centre (Γ point) and of the L valleys, respectively. $E_{v,lh}$ and $E_{v,hh}$ are the energies of the tops of the light-hole and heavy-hole valence bands, respectively. The $Ge_{0.94}Sn_{0.06}/Si_{0.16}Ge_{0.84}$ quantum well on (001)-oriented relaxed $Si_{0.1}Ge_{0.9}$ has type-I alignment at the zone centre. Carriers are confined inside the $Ge_{0.94}Sn_{0.06}$ well.

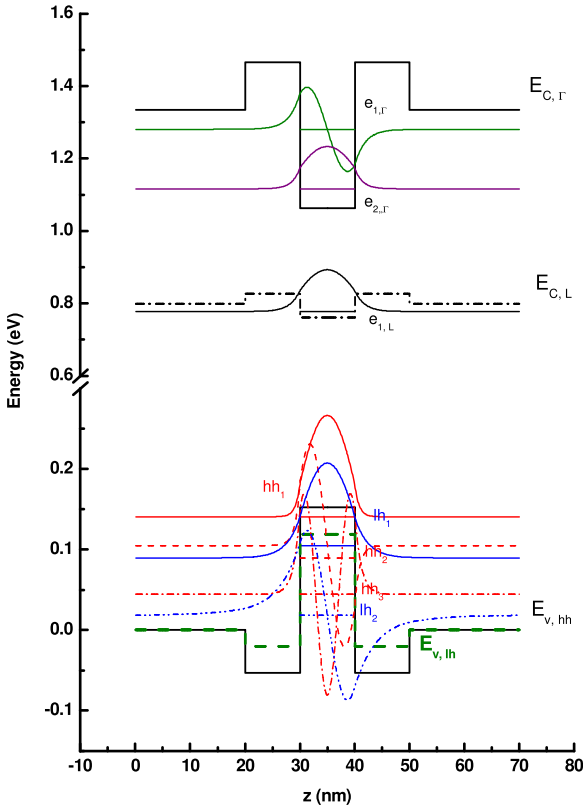

FIG. 5. Band alignment, wave functions, and energy levels for electrons, light holes (blue color) and heavy holes (red color) for the $Si_{0.16}Ge_{0.84}/Ge_{0.94}Sn_{0.06}/Si_{0.16}Ge_{0.84}$ quantum well strain on relaxed $Si_{0.10}Ge_{0.90}$. The origin of energy is taken at the bottom of the Ge quantum well. Note the type-I alignment both for L and Γ gaps.

$$|M_b|^2 = \frac{m_0^2 E_g(E_g+\Delta)}{12m_e\left(E_g+\frac{2}{3}\Delta\right)}. \tag{26}$$

In which m_e is the electron effective mass and Δ is the spin orbit split-off energy.

In Eq. (25), $F(\hbar\omega_0-\hbar\omega)$ is the Gaussian line shape function defined as

$$F(\hbar\omega_0-\hbar\omega) = \frac{1}{\sqrt{\Pi}\delta}\exp\left[-(\hbar\omega_0-\hbar\omega)^2/\delta^2\right], \tag{27}$$

with

$$\hbar\omega_0 = E+E_g+E_{ei}+E_{hj} \text{ and } \delta = \frac{h}{\tau(\ln 2)^{-1/2}}, \tag{28}$$

where τ is the interband relaxation time. The energy dependence of the energy- and polarization dependent transition matrix elements[46] are given by the following equations:

$$M(E) = \frac{3}{4}(1+\cos^2\theta) = \frac{3}{4}\left(1+\frac{E_{ei}+E_{hj}}{E_{ei}+E_{hj}+E}\right)$$
(for electron to heavy hole transitions), (29)

$$M(E) = \frac{1}{4}(5-3\cos^2\theta) = \frac{1}{4}\left(5-3\frac{E_{ei}+E_{hj}}{E_{ei}+E_{hj}+E}\right)$$
(for electron to light hole transitions), (30)

where θ is the angle of the electron wave vector with respect to the z axis (normal to the well plane). The polarization is assumed to be parallel to the plane of the layers (TE-mode).

To obtain the absorption coefficient due to electronic transitions inter conduction and valence bands, described in Eq. (25), one needs to know the band structures and the corresponding wave functions. The one band k·p method is useful technique for analyzing the conduction and the valence band structures near the band edges. For simplicity, we assume that the conduction and the valence bands are decoupled, which is a good approximation for IV-IV semiconductors.[49] By solving the potential problem numerically for the conduction band and the valence band, one can get confined state energies and wave functions for electrons and holes. Then, one can calculate the absorption coefficient of the type-I $Si_{0.16}Ge_{0.84}/Ge_{0.94}Sn_{0.06}$ quantum well strain on relaxed $Si_{0.10}Ge_{0.90}$ buffer. Results of our computation of the absorption coefficient spectra in this modeled with 10 nm $Ge_{0.94}Sn_{0.06}$ well thick at zero bias are shown in Figure 6. The peaks observed at the spectrum of absorption are in part ascribed to the interband transition series consisting of hh_n-L_n, lh_n-L_n, hh_n-$c\Gamma_n$, lh_n-$c\Gamma_n$, 2D-2D, and 2D-3D. In the inset, the conduction and valence band profiles, electron and hole confined states and the transitions visible in the absorption coefficient spectra are also shown. The room temperature spectrum shows the typical staircase line shape proportional to the combined density of states in direct-gap type I QWs. In fact, as demonstrated in Ref. 50, the near-edge absorption spectrum of GeSn with Ge-rich QWs is dominated by transitions involving heavy- and light hole valence band states and conduction band states at the Γ point, spatially confined by a type I profile. In the same spatial region, L conduction band states are also present. They have lower energy with respect to the conduction band states at the Γ point. Nevertheless, the role of L states in the near-edge absorption region can be neglected due to the low oscillator strength related to the k-indirect nature of the Γ-L transitions.

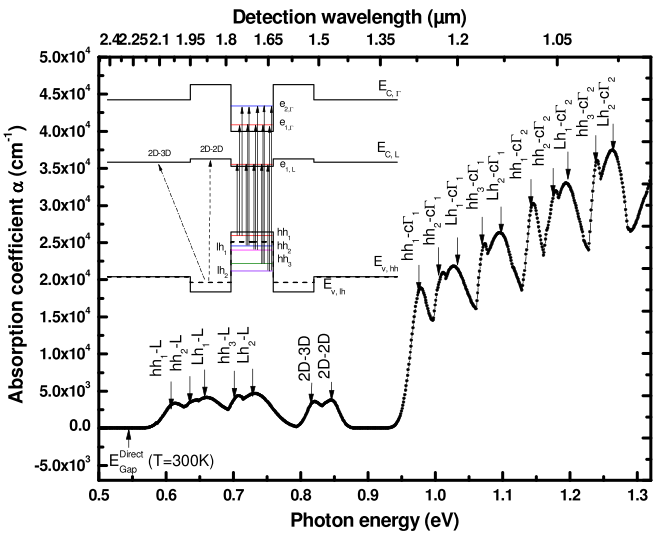

FIG. 6. Theoretical absorption coefficient spectra of $Ge_{0.94}Sn_{0.06}/Si_{0.16}Ge_{0.84}$ QW at room temperature. The peaks correspond to the hh_n-L_n, lh_n-L_n, hh_n-$c\Gamma_n$, lh_n-$c\Gamma_n$, 2D-2D, and 2D-3D transitions. In the inset, the conduction and valence band edge profiles, electron, hole confined states and the transitions visible in the spectra of absorption are also shown.

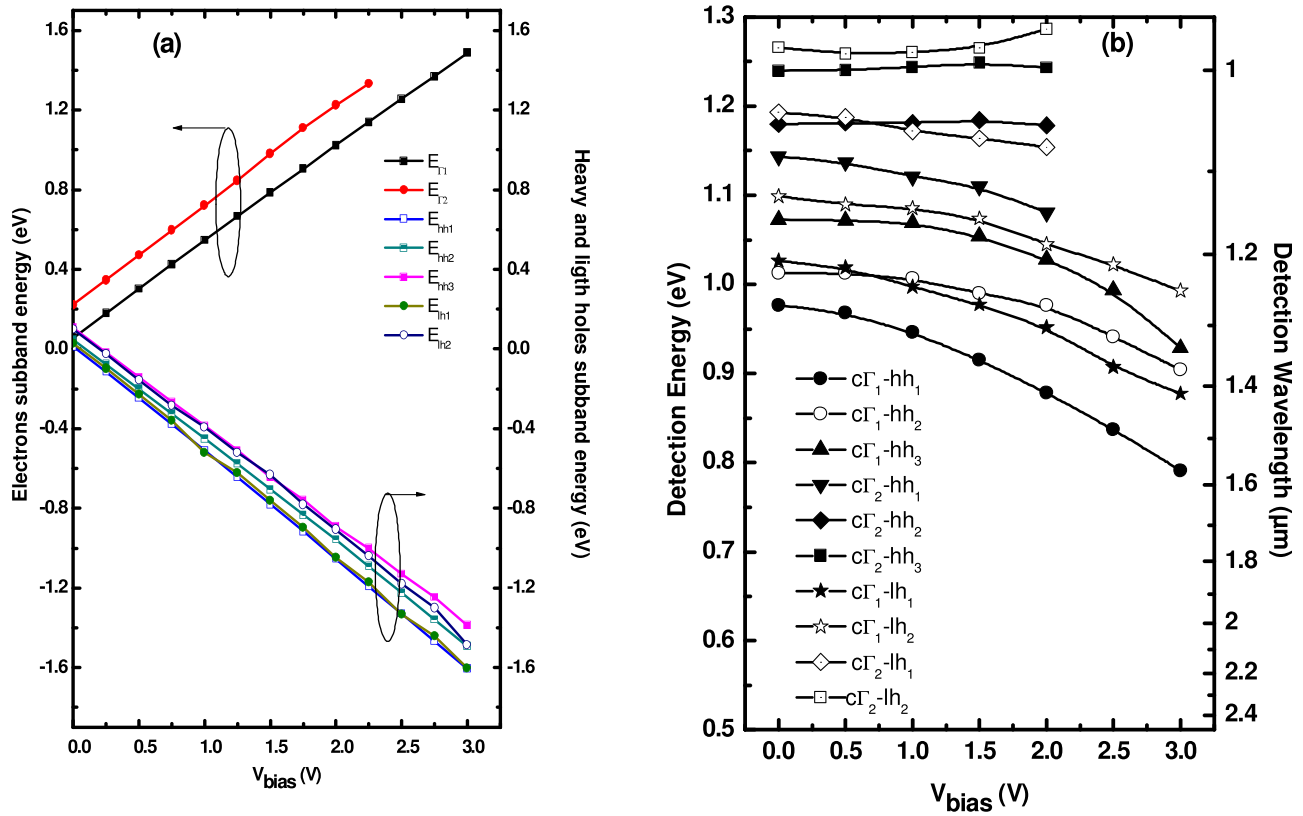

FIG. 7. (a) Heavy (light) hole (left-hand scale) and electron at the Γ point (right-hand scale) confinement energies, (b) the detection energies of hh_n-$c\Gamma_1$, lh_n-$c\Gamma_1$ and hh_n-$c\Gamma_2$, lh_n-$c\Gamma_2$ transitions of a 10 nm-thick $Si_{0.16}Ge_{0.84}$/10 nm-thick $Ge_{0.94}Sn_{0.06}$/10 nm-thick $Si_{0.16}Ge_{0.84}$ strained quantum well embedded in relaxed $Si_{0.10}Ge_{0.90}$ buffer versus bias voltage.

To understand quantum-confined Stark effect in a GeSn/SiGe quantum-well structure, we consider the influence of an applied electric on the energy levels. In our model, the bias voltage appears as a shift of the Fermi-energy as bias is taken into account within the Schrödinger equation that has been corrected by including eF_z, where F_z is the perpendicular external electric field. This leads to external field-dependence solutions of the energies for all subbands and their related wave functions. The effects of charges (close to the Fermi level) and bias potential could be included via the simultaneous resolution of the Poisson equation[51] but this is not done in the present work. In Figures 7(a) and 7(b), we report the confinement as well as the detection energies (and wavelengths) for the interband transition series consisting hh_n-$c\Gamma_1$, lh_n-$c\Gamma_1$, hh_n-$c\Gamma_2$, and lh_n-$c\Gamma_2$ as a function of an applied voltage. In fact, the transition energies between the electron and holes levels decrease with applied voltage varying from 0 to 3 V. The calculation proved that the quantum-well thickness is the dominant parameter (together with strain) in setting the amount of quantum-detection energies. Accordingly, in the range of wavelength on which the quantum confined Stark effect settings will be observed. As known, alloying of Ge with Sn gives great quantum-confinement energies and leads to small quantum-confined Stark effect changes in these energies. For 10 nm width $Ge_{0.94}Sn_{0.06}$ QW, the large shift observed in Figure 7 is due to the corresponding overlap integral between the electron and hole wave functions, after that the absorption strength will fall off very quickly with bias voltage and the behavior will become progressively more similar to that of Ge bulk materials.[52] Figure 8 illustrates the results of our computation of the absorption coefficient spectra for the same heterostructure for bias voltages from zero up to 3 V at room temperature. When the electric field is increased, two main characteristics of GeSn/SiGe QW are observed, the hh_1-$c\Gamma_1$ absorption peak, which coincides with 1.27 μm (0.977 eV), is shifted toward larger wavelengths and the absorption edge is gradually attenuated. This shift can be

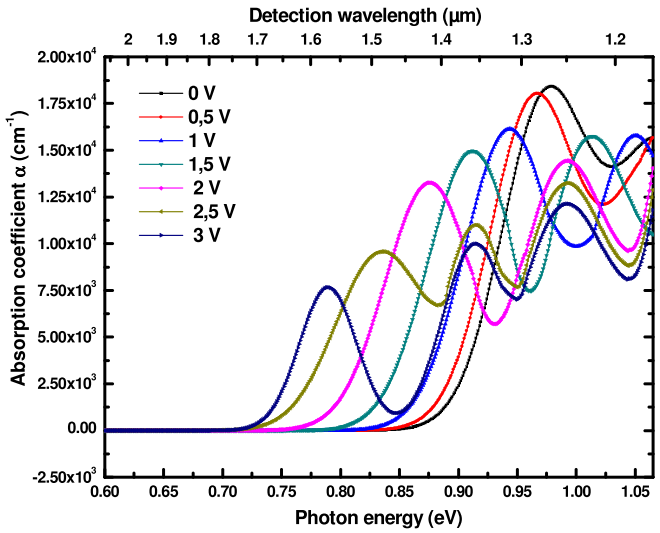

FIG. 8. Theoretical absorption coefficient spectra of $Ge_{0.94}Sn_{0.06}$/$Si_{0.16}Ge_{0.84}$ (10-nm $Ge_{0.94}Sn_{0.06}$ well and 10-nm $Si_{0.16}Ge_{0.84}$ barrier) quantum well on a relaxed $Si_{0.1}Ge_{0.9}$ buffer at room temperature versus bias voltage.

interpreted as a combination of strain and quantum confinement energies. Similarly, we note that the other transitions occur at a lower wavelength ($<1.55\ \mu$m) at this applied bias voltage. Furthermore, it is found that, even at low Sn concentration, the absorption coefficients are higher than those in comparable pure-Ge device designs (Ref. 32 and references therein). Moreover, an increase of Sn content shifts the absorption coefficient curve to higher wavelengths compared with pure Ge.[53,54] Finally, we find that the GeSn alloy is promising for sensitive devices application as well as Germanium.

IV. CONCLUSION

In conclusion, we have theoretically studied the group-IV semiconductor in which the GeSn relaxed alloys has a direct band gap for 6% α-Sn. Our investigation predicts, at room temperature, a direct band gap for strained GeSn/Ge (001) and $GeSn/Si_{0.1}Ge_{0.9}(001)$ semiconductor structures at a Sn-fraction higher than 15.3% and 20%, respectively. The active region has a quantum well structure formed $Ge_{0.94}Sn_{0.06}$ separated by $Si_{0.16}Ge_{0.84}$ barriers embedded in relaxed $Si_{0.10}Ge_{0.90}$ layer. These alloy compositions of both active and barriers layers are determined to yield a type-I band alignment and direct transitions. The absorption spectra as well as the detection energies dependency on the applied voltage from zero up to 3 V have been instigated at room temperature. We explored some important properties of $Ge_{1-x}Sn_x$ alloys useful for optoelectronic applications. Specifically, we have studied band structure and effective masses of GeSn/SiGe. We have found a direct interband absorption for strain $Ge_{0.94}Sn_{0.06}/Si_{0.16}Ge_{0.84}$ quantum well on a $Si_{0.10}Ge_{0.90}$ relaxed buffer. The bias voltage shifts the absorption edge of $Ge_{0.94}Sn_{0.06}$ from 0.977 eV to 0.8 eV. This shows the large potential of these structures, for example, to achieve high performance electro-absorption modulators operating at 1.55 μm.

[1]J. Wang and S. Lee, Sensors **11**, 696 (2011).
[2]P. K. Basu, N. R. Das, B. Mukhopadhyay, G. Sen, and M. K. Das, Opt. Quantum Electron. **41**, 567 (2009).
[3]Y. H. Ahn and J. Park, Appl. Phys. Lett. **91**, 162102 (2007).
[4]P. H. Lim, S. Park, Y. Ishikawa, and K. Wada, Opt. Express **17**, 16358 (2009).
[5]J. Liu, X. Sun, R. Camacho-Aguilera, L. C. Kimerling, and J. Michel, Opt. Lett. **35**, 679–681 (2010).
[6]F. Zhang, V. H. Crespi, and P. Zhang, Phys. Rev. Lett. **102**, 156401 (2009).
[7]Y. Huo, H. Lin, R. Chen, M. Makarova, Y. Rong, M. Li, T. I. Kamins, J. Vuckovic, and S. H. Harris, Appl. Phys. Lett. **98**, 011111 (2011).
[8]D. Nam, D. Sukhdeo, A. Roy, K. Balram, S.-L. Cheng, K. C.-Y. Huang, Z. Yuan, M. Brongersma, Y. Nishi, D. Miller, and K. Saraswat, Opt. Express **19**(27), 25866 (2011).
[9]G. Capellini, G. Kozlowski, Y. Yamamoto, M. Lisker, C. Wenger, G. Niu, P. Zaumseil, B. Tillack, A. Ghrib, M. de Kersauson, M. El Kurdi, P. Boucaud, and T. Schroeder, J. Appl. Phys. **113**, 013513 (2013).
[10]J. R. Jain, A. Hryciw, T. M. Baer, D. A. Miller, M. L. Brongersma, and R. T. Howe, Nature Photon. **6**, 398 (2012).
[11]Y. H. Kuo, Y. K. Lee, Y. Ge, S. Ren, J. E. Roth, T. I. Kamins, D. A. B. Miller, and S. Harris, Nature (London) **437**, 1334 (2005).
[12]G. He and H. A. Atwater, Phys. Rev. Lett. **79**, 1937 (1997).
[13]J. Mathews, R. T. Beeler, J. Tolle, C. Xu, R. Roucka, J. Kouvetakis, and J. Menéndez, Appl. Phys. Lett. **97**, 221912 (2010).
[14]V. R. D'Costa, C. S. Cook, A. G. Birdwell, C. L. Littler, M. Canonico, S. Zollner, J. Kouvetakis, and J. Menendez, Phys. Rev. B **73**, 125207 (2006).
[15]W.-J. Yin, X.-G. Gong, and S.-H. Wei, Phys. Rev. B **78**, 161203 (2008).
[16]S. Gupta, B. M. Köpe, Y. Nishi, and K. C. Saraswat, J. Appl. Phys. **113**, 073707 (2013).
[17]J. D. Sau and M. L. Cohen, Phys. Rev. B **75**, 045208 (2007).
[18]S. Gupta, R. Chen, B. Magyari-Köpe, H. Lin, B. Yang, A. Nainani, J. S. Harris, and K. C. Saraswat, in *Proceedings of the IEEE International Electron Devices Meeting* (Institute of Electrical and Electronics Engineering Proceedings, 2011) p. 398.
[19]S. Gupta, B. Vincent, D. Lin, M. Gunji, A. Firrincieli, F. Gencarelli, B. Magyari-Köpe, B. Yang, B. Douhard, J. Delmotte, A. Franquet, M. Caymax, J. Dekoster, Y. Nishi, and K. C. Saraswat, in *Proceedings of the IEEE VLSI Technology Symposium* (Institute of Electrical and Electronics Engineering Proceedings, 2012), p. 95.
[20]I. S. Yu, T. H. Wu, K. Y. Wu, H. H. Cheng, V. I. Mashanov, A. I. Nikiforov, O. P. Pchelyakov, and X. S. Wu, AIP Adv. **1**, 042118 (2011).
[21]A. A. Tonkikh, C. Eisenschmidt, V. G. Talalaev, N. D. Zakharov, J. Schilling, G. Schmidt, and P. Werner, Appl. Phys. Lett. **103**, 032106 (2013).
[22]S. W. Chang and S. L. Chuang, IEEE J. Quantum Electron. **43**, 249–256 (2007).
[23]G. E. Chang, S. W. Chang, and S. L. Chuang, Opt. Express **17**, 11246 (2009).
[24]G. E. Chang, S. W. Chang, and S. L. Chuang, IEEE J. Quantum Electron. **46**, 1813–1820 (2010).
[25]G. Sun, R. A. Soref, and H. H. Cheng, J. Appl. Phys. **108**, 033107 (2010).
[26]G. Sun, R. A. Soref, and H. H. Cheng, Opt. Express **18**, 19957 (2010).
[27]P. Moontragoon, N. Vukmirovic, Z. Ikonic, and P. Harrison, IEEE J. Sel. Top. Quantum Electron. **16**, 100–105 (2010).
[28]J. Mathews, R. Roucka, J. Xie, S.-Q. Yu, J. Menéndez, and J. Kouvetakis, Appl. Phys. Lett. **95**, 133506 (2009).
[29]J. Werner, M. Oehme, M. Schmid, M. Kaschel, A. Schirmer, E. Kasper, and J. Schulze, Appl. Phys. Lett. **98**, 061108 (2011).
[30]S. Su, B. Cheng, C. Xue, W. Wang, Q. Cao, H. Xue, W. Hu, G. Zhang, Y. Zuo, and Q. Wang, Opt. Express **19**, 6400–6405 (2011).
[31]G.-E. Chang and C.-O. Chang, IEEE J. Quantum Electron. **48**, 533 (2012).
[32]N. Yahyaoui, N. Sfina, J.-L. Lazzari, A. Bournel, and M. Said, Eur. Phys. J. B **86**, 59 (2013).
[33]V. R. D'Costa, Y.-Y. Fang, J. Tolle, J. Kouvetakis, and J. Menéndez, Thin Solid Films **518**, 2531 (2010).
[34]W. A. Harrison, *Electronic Structure and the Properties of Solids* (Freeman, San Francisco, CA, 1980).
[35]J. R. Chelikowsky and M. L. Cohen, Phys. Rev. B **14**, 556–582 (1976).
[36]N. Bouarissa, Phys. Lett. A **245**, 285–291 (1998).
[37]S. J. Lee, T. S. Kwon, K. Nahm, and C. K. Kim, J. Phys.: Condens. Matter **2**, 3253 (1990).
[38]H. Pérez Ladrón de Guevara, A. G. Rodríguez, H. Navarro-Contreras, and M. A. Vidal, Appl. Phys. Lett. **91**, 161909 (2007).
[39]R. People and S. K. Sputz, Phys. Rev. B **41**, 8431 (1990).
[40]V. R. D'Costa, Y. Fang, J. Mathews, R. Roucka, J. Tolle, J. Menéndez, and J. Kouvetakis, Semicond. Sci. Technol. **24**, 115006 (2009).
[41]P. Y. Yu and M. Cardona, *Fundamentals of Semiconductors: Physics and Materials Properties* (Springer, Berlin, 1996).
[42]N. Sfina, J. Lazzari, J. Derrien, F. A. d'Avitaya, and M. Said, Eur. Phys. J. B **48**, 151 (2005).
[43]G. Grzybowski, R. T. Beeler, L. Jiang, D. J. Smith, J. Kouvetakis, and J. Menendez, Appl. Phys. Lett. **101**, 072105 (2012).
[44]B. Vincent, F. Gencarelli, H. Bender, C. Merckling, B. Douhard, D. H. Petersen, O. Hansen, H. H. Henrichsen, J. Meersschaut, W. Vandervorst, M. Heyns, R. Loo, and M. Caymax, Appl. Phys. Lett. **99**, 152103 (2011).
[45]R. Chen, Y.-C. Huang, S. Gupta, A. C. Lin, E. Sanchez, Y. Kim, K. C. Saraswat, T. I. Kamins, and J. S. Harris, J. Cryst. Growth **365**, 29 (2013).
[46]M. Yamanishi and I. Suemune, Jpn. J. Appl. Phys., Part 1 **23**, 35 (1984).
[47]Y. Kan, M. Yamanishi, Y. Usami, and I. Suemune, IEEE J. Quantum Electron. **22**, 1837 (1986).
[48]H. C. Casey, Jr. and M. B. Panish, *Heterostructure Lasers, Part A: Fundamental*, (Academic Press, New York, 1978), Chap. 3, p 150.
[49]V. Chakraborty, B. Mukhapadhyay, and P. K. Basu, Physica E **50**, 67 (2013).
[50]M. Bonfanti, E. Grilli, M. Guzzi, M. Virgilio, G. Grosso, D. Chrastina, G. Isella, H. von Känel, and A. Neels, Phys. Rev. B **78**, 041407 (2008).
[51]F. Ben Zid, A. Bhouri, H. Mejri, R. Tlili, M. Said, J.-L. Lazzari, F. Arnaud D'Avitaya, and J. Derrien, J. Appl. Phys. **91**, 9170 (2002).
[52]D. S. Chemla, D. A. B. Miller, P. W. Smith, A. C. Gossard, and W. Wiegmann, IEEE J. Quantum Electron. **20**, 265 (1984).
[53]M. Oehme, M. Schmid, M. Kaschel, M. Gollhofer, D. Widmann, E. Kasper, and J. Schulze, Appl. Phys. Lett. **101**, 141110 (2012).
[54]A. Gassenq, F. Gencarelli, J. Van Campenhout, Y. Shimura, R. Loo, G. Narcy, B. Vincent, and G. Roelkens, Opt. Express **20**, 27297 (2012).